Naval Research Laboratory
Washington, DC 20375-5320

NRL/7230/MR—2022/3

Macro- and Micro-Physical Sensitivities of Coupled Atmosphere-Ocean to Polarized Space Observations

AHMED M. EL-HABASHI

Coastal and Ocean Remote Sensing Branch
Remote Sensing Division

December 22, 2022

REPORT DOCUMENTATION PAGE

Form Approved
OMB No. 0704-0188

1. REPORT DATE *(DD-MM-YYYY)*	**2. REPORT TYPE**	**3. DATES COVERED** *(From - To)*
22-12-2022	NRL Memorandum Report	08/2021 – 08/2022

4. TITLE AND SUBTITLE

Macro- and Micro-Physical Sensitivities of Coupled Atmosphere-Ocean to Polarized Space Observations

5a. CONTRACT NUMBER

5b. GRANT NUMBER

5c. PROGRAM ELEMENT NUMBER
NISE

6. AUTHOR(S)

Ahmed M. El-Habashi

5d. PROJECT NUMBER

5e. TASK NUMBER

5f. WORK UNIT NUMBER
N20P

7. PERFORMING ORGANIZATION NAME(S) AND ADDRESS(ES)

Naval Research Laboratory
4555 Overlook Avenue, SW
Washington, DC 20375-5320

8. PERFORMING ORGANIZATION REPORT NUMBER

NRL/7230/MR--2022/3

9. SPONSORING / MONITORING AGENCY NAME(S) AND ADDRESS(ES)

Naval Research Laboratory
4555 Overlook Avenue, SW
Washington, DC 20375-5320

10. SPONSOR / MONITOR'S ACRONYM(S)
NRL

11. SPONSOR / MONITOR'S REPORT NUMBER(S)

12. DISTRIBUTION / AVAILABILITY STATEMENT

DISTRIBUTION STATEMENT A: Approved for public release; distribution is unlimited.

13. SUPPLEMENTARY NOTES
Karles Fellowship

14. ABSTRACT

This document contains a summary of the research conducted by the author as part of the The Jerome and Isabella Karle Distinguished Scholar Fellowship Program. The research period covered is August 16, 2021 through August 15, 2022.

15. SUBJECT TERMS

Aerosol-ocean micro-physics
Polarimetric airborne imaging
Vector radiative transfer
Polarized remote sensing

16. SECURITY CLASSIFICATION OF:			**17. LIMITATION OF ABSTRACT**	**18. NUMBER OF PAGES**	**19a. NAME OF RESPONSIBLE PERSON**
a. REPORT	**b. ABSTRACT**	**c. THIS PAGE**			Ahmed El-Habashi
U	U	U	U	16	**19b. TELEPHONE NUMBER** *(include area code)* (202) 767-0043

This page intentionally left blank.

CONTENTS

FIGURES

TABLES

EXECUTIVE SUMMARY

This report presents multiple significant research that has been conducted during my 12-month Karle fellowship. The research efforts were distributed between my own independent research and several other collaborative research with different NRL employees and external collaborators. The independent research builds upon the work performed during my National Research Council (NRC) postdoctoral Associateship at NRL. The independent research included:

1. Polarimetric Remote Sensing Analysis using:
    a. Airborne multi-spectral hyper-angular polarimetric imager: VICO
    b. Vector Radiative Transfer Theory
2. Coupled Atmosphere-Ocean Micro-physics Sensitivities to the Polarized Space Observations
    a. Investigated the impact of small hydrosol particles on polarized observations
    b. Performed Jacobian sensitivity analysis of aerosol and hydrosol microphysics.

Other progress made on multiple collaborative research included:

1. Hydrosol Scattering Matrix Inversion Across a Fresnel Boundary [1].
2. Particles discrimination from polarization (NRL).
3. Arctic and Anti-Arctic ocean characterizations (NASA).
    a. Analyzed Inherent Optical Properties IOPs in the polar regions.
4. The importance of particle disaggregation on biogeochemical flux predictions (NSF).
    a. Measured Size distribution and in focus images of particles suspended in water.
    b. Characterized Inherent Optical Properties of the studied regions.
    c. Performed hyperspectral polarimetric measurements.
5. Characterized the hyperspectral Inherent Optical Properties, IOP of seven microplastics assemblages (synthetic polymers), commonly found in the marine environment.

Although I contributed significantly to these research topics during my Karle fellowship, results are not included in this report. Results from the collaborative research are preliminary and expected to be published in the near future and in the cited reference.

This page intentionally left blank.

MACRO- AND MICRO-PHYSICAL SENSITIVITIES OF COUPLED ATMOSPHERE-OCEAN TO POLARIZED SPACE OBSERVATIONS

1. INTRODUCTION

Over the last several decades, space-based measurements of the ocean relied on measurements of a single-view multi-spectral radiance. First single-viewed ocean color instrument was the Coastal Zone Color Scanner Experiment (CZCS) launched into space in 1978. Following the CZCS, a fleet of single-view satellite sensors such as SeaWiFS, MODIS, VIIRS, MERIS, OLCI, and GOCI were launched, providing a continuous data record of the global ocean over the past two decades. The Multi-angle Imaging SpectroRadiometer (MISR) was launched in 1999, to observe Earth's climate with cameras pointed at nine different angles. These instruments provided a wealth of ocean information from space; however, the retrieved data accuracy was limited. A higher retrieval accuracy and additional products are needed for better characterization of the aerosol and hydrosol constituents from spaceborne and airborne remote sensing. Recent work on polarimetry has shown that it is capable of providing higher retrieval accuracies and additional information on the micro-physical and macro-physical properties of aerosol and hydrosol particles, which are difficult to infer from the scalar scattered radiation observed by the current ocean color instruments [2, 3]. Polarization is sensitive to the aerosol and hydrosol particles composition (complex refractive index), size, and shape. The polarized light reflected from the sea surface contains useful information on the sea state. Current and future remote sensing polarimeters can measure the degree of linear polarization to an absolute accuracy < 0.2%. The radiative transfer codes used to analyze these polarimetric measurements can provide an accuracy that exceeds state-of-the-art polarimeters < 0.2%. It is expected that the polarized remote sensing will provide an accurate atmospheric correction that can lead to improved aerosol and hydrosol products [4].

2. POLARIMETRIC REMOTE SENSING

2.1 Airborne multi-spectral hyper-angular polarimetric imager: VICO

The remote sensing instrument used is the aircraft-based Versatile Imager for the Coastal Ocean (VICO) developed by the Naval Research Laboratory (NRL). VICO is designed to collect hyper-angular linear polarization at four visible and NIR spectral channels in an imaging mode, as done with the HARP2/PACE instrument, but with higher polarimetric accuracy, similar to the SPEXone/PACE instrument. The accuracy level in the measured VICO DoLP is better than 0.25% [5] with sufficiently small angular resolution (~0.12°). In addition, VICO is a pointable instrument (gimbaled system), which makes it suitable for ocean color applications by allowing the measurement of the polarized light field in and off the principle-viewing plane. VICO design and specification make it a retrieval-capable instrument providing a better characterization of the aerosol and hydrosol properties. The polarimetric dataset acquired by the instrument is expected to be utilized to verify data processing and validate algorithm performance for spaceborne polarimeters such as HARP2 and SPEXone on the forthcoming PACE observatory. The design, fabrication, calibration, and airborne deployment methodologies of VICO (Table 1 and Fig. 2 .) are described in more detail by Bowles et al. and El-Habashi et al [4, 5].

Manuscript approved November 21, 2022.

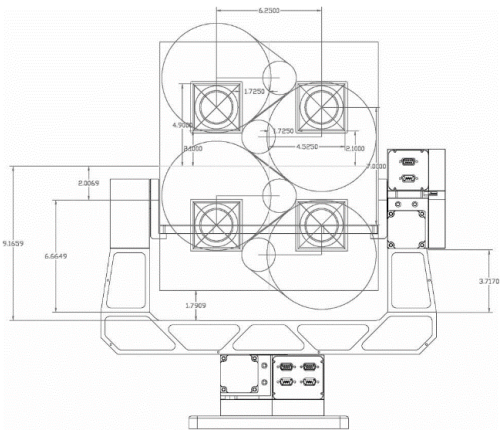

Fig. 1 VICO schematic diagram showing four cameras indicated by the X's with tear drop-shaped filter wheels mounted on a plate. Cameras are mounted onto a stage. The rotation of the U-shaped yoke moves the FOV in the general direction of the area of interest.

VICO is designed to record the polarized radiance at 0°, 45°, 90° and 135° relative to the vertical. Radiances are recorded in imaging mode and at four narrow spectral bands centered at 435, 550, 625, and 750 nm. The polarized radiance is used to compute the linear Stokes parameters of the incoming light observed at the aircraft altitude as follows (Eq. 1):

$$\bar{S}^{obs} = \begin{bmatrix} I \\ Q \\ U \end{bmatrix}^{obs} = \begin{bmatrix} 0.5(I_0 + I_{90} + I_{45} + I_{135}) \\ I_0 - I_{90} \\ I_{45} - I_{135} \end{bmatrix} \quad \textbf{(1)}$$

where I is to the total radiance. Q and U specify the state of linear polarization to the local meridional plane of reference.

The bi-directional reflectance ρ, the degree of linear polarization, $DoLP$, and the angle of linear polarization, $AoLP$, are calculated using the linear Stokes parameters defined in Eq. 1 as follows:

$$\begin{bmatrix} \rho \\ DoLP \\ AoLP \end{bmatrix}^{Z} = \begin{bmatrix} \rho_u + \rho_p \\ \sqrt{Q^2 + U^2}/I \\ 0.5 \times \tan^{-1}(U/Q) \end{bmatrix} \quad \textbf{(2)}$$

The bi-directional reflectance, ρ, is a linear combination of the un-polarized ρ_u and a polarized ρ_p components. The bi-directional reflectance components are the total radiance and the linearly polarized radiance, each scaled by the solar reflected radiation.

$$\begin{bmatrix} \rho_u \\ \rho_p \end{bmatrix} = \frac{\pi r_0^2}{\mu_0 F_0} \times \begin{bmatrix} (1 - DoLP) \times I \\ DoLP \times I \end{bmatrix} \quad \textbf{(3)}$$

where the extraterrestrial solar irradiance [6], F_0, the cosine of solar zenith angle, μ_0, and the Sun-Earth distance correction factor, r_0^2, describes the solar radiation at the top of the atmosphere, TOA. Note that all parameters in Eq. 1-3 are spectrally and geometrically dependent, $(\theta_v, \varphi_v, \lambda)$ and can be calculated at any given level, Z, for each studied case.

The use of the reflectance and DoLP parameters is to represent the at-sensor's incoming unpolarized and polarized light independently from the solar radiation, and the choice of a reference plane for the Q and U parameters. Along with that, the error level in DoLP and AoLP parameters is less since these quantities are derived from calibrated radiance ratios at the same pixel. This ratio also cancels out the systematic errors associated with integrating sphere radiance level. Similarly, linear Stokes parameters normalized by the total radiance (Q/I and U/I) are unaffected by these particular errors. The accuracy of VICO is better than 0.25% for the $DoLP$ [5].

2.2 Vector Radiative Transfer Theory

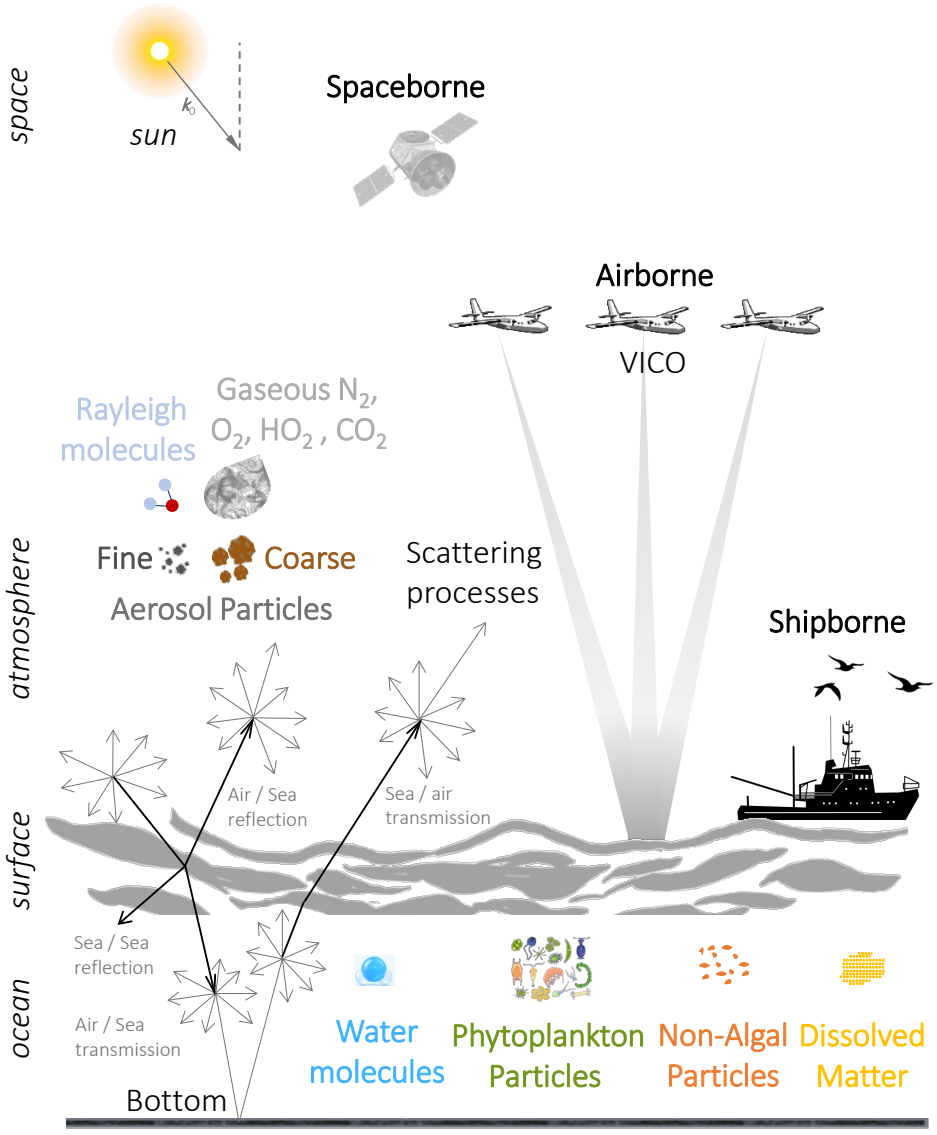

Fig. 2 Shows the Atmosphere-Ocean System AOS layers used for Radiative Transfer RT computations illustrating the interactions of light on the sea surface interface, in the atmosphere and ocean, and on the bottom of the sea

Vector Radiative transfer models (VRT) are necessary to simulate the polarimetric quantities observed by a satellite or airborne sensors under various atmospheric and oceanic conditions. In this study, the Ocean Successive Orders with Atmosphere - Advanced (OSOAA) vector radiative transfer code was used to model the airborne and shipborne field measurement. The model computes the complete radiance

field and the linear polarization state in a coupled ocean-atmosphere system. OSOAA calculates the radiative parameters for each component of the environment, assuming a set of plane-parallel homogeneous layers throughout the atmospheric and marine profiles [7]. The code numerically calculates the contribution of each scattering order based on the successive orders of scattering method [8, 9]. A detailed description of the code is presented in [10].

OSOAA model was used in a forward model to compute radiance and polarization for various viewing angles at the aircraft and top of the atmosphere levels. Scattering and absorption by molecules were characterized by their optical depths and depolarization ratio. The radiative properties of aerosol and hydrosol particles were described [4] by the single scattering albedo, optical depth, and single- scattering Mueller matrix. The coupled atmosphere-ocean system is illustrated in Fig. 2.

After the first run of the VRT simulations, the optical parameters of aerosol and hydrosol were used, as initialized optimization variables for new simulation runs. The new runs were made to get the best possible VRT optical closure between the simulation and airborne observation. To obtain an optimal closure, we considered a multi-objective optimization method in which all the objectives (The simulated radiance field and polarization state at different wavelengths and different viewing angles) are improved simultaneously. Various aerosol and hydrosol optical properties were optimized using the gradient–based optimization techniques. The choice of the optimization parameters was based on the gradients of the objectives that helped moving the optical closure in the non–dominated (i.e. the most promising) improving directions. In particularly, the microphysical properties (such as the complex refractive index spectra and the volumetric radii) of the aerosol fine mode were adjusted for both of the selected cases. The chlorophyll-a amount, and the dissolved and detritus absorptions of the open ocean case were slightly adjusted. The optical closure results showed that the radiance and the linearly polarized light of the observed scenes matches well the VRT simulations. The optical closure was consistent at different wavelengths and at various viewing angles (Fig. 3 left column), thus illustrating that light scattering and absorbing features of the atmosphere-ocean systems are well reproduced by simulations.

3. ATMOSPHERE-OCEAN MICRO-PHYSICS SENSITIVITIES TO POLARIZED SPACE OBSERVATIONS

Polarimetric remote sensing provide both higher retrieval accuracy and additional information on the determination of the optical and micro-physical properties of suspended particulates [11, 12]. In this section, we utilize airborne polarimetry and the vector radiative transfer modeling to determine the radiance and linear polarization sensitivities to the atmosphere-ocean micro-physics.

3.1 Impact of super- and sub-micron hydrosol particles on polarized observations

Backscattering of light by particles is an important input for the ocean inverse problem. The understanding of what particles generate the ocean backscattering signal is incomplete and often results to unaccounted backscattering in the ocean signal. The unaccounted backscattering results in an inaccurate retrieval of the ocean parameters. Organelli et. al. 2018 suggested that most of the signal comes from particles >1 μm. The study predicted the measured backscattering using optical model that relies on coated spheres [13]. Zhang et. al. 2020 showed that backscattering by submicron particles in clear ocean waters is significant [14]. The study also suggests that the backscattering by submicron particles forms a background that is independent of the backscattering by larger particles. Indeed, the backscattering process is associated with very small particles (Morel 1991) , and the scattering process is associated with the larger particles (a factor of 10) such as the algal cells. Nonetheless, the origin of the backscattering in the ocean is not clear and can be attributed to size, the structural complexity of particles or both.

We utilized the polarimetric optical closure to study the impact of hydrosol particles sizes on the observed unpolarized and linearly polarized angular spectrum at 1500-meter altitude. The size sensitivity of the hydrosol particles was performed using multiple sets of the VRT simulation. First simulation set is the polarimetric optical closure which uses the atmospheric and oceanic conditions measured at the time of the VICO imaging. Other simulation sets were made the same but with different hydrosol particles size limits 0.3, 0.5, 1, 50 μm respectively. A considerable spectral-angular variation in the optical closure were found with the greatest variation observed at the green-red bands. The variations in the matched total reflectance ρ, Degree of Linear Polarization *DoLP*, Angle of Linear Polarization *AoLP* ranged from 0.01 to -0.04 sr^{-1}, -1 to -20 %, 7 to -3 ° respectively. Figure 3 illustrate the sensitivity of ρ, *DoLP* and *AoLP* to super- and sub-micron hydrosol particles.

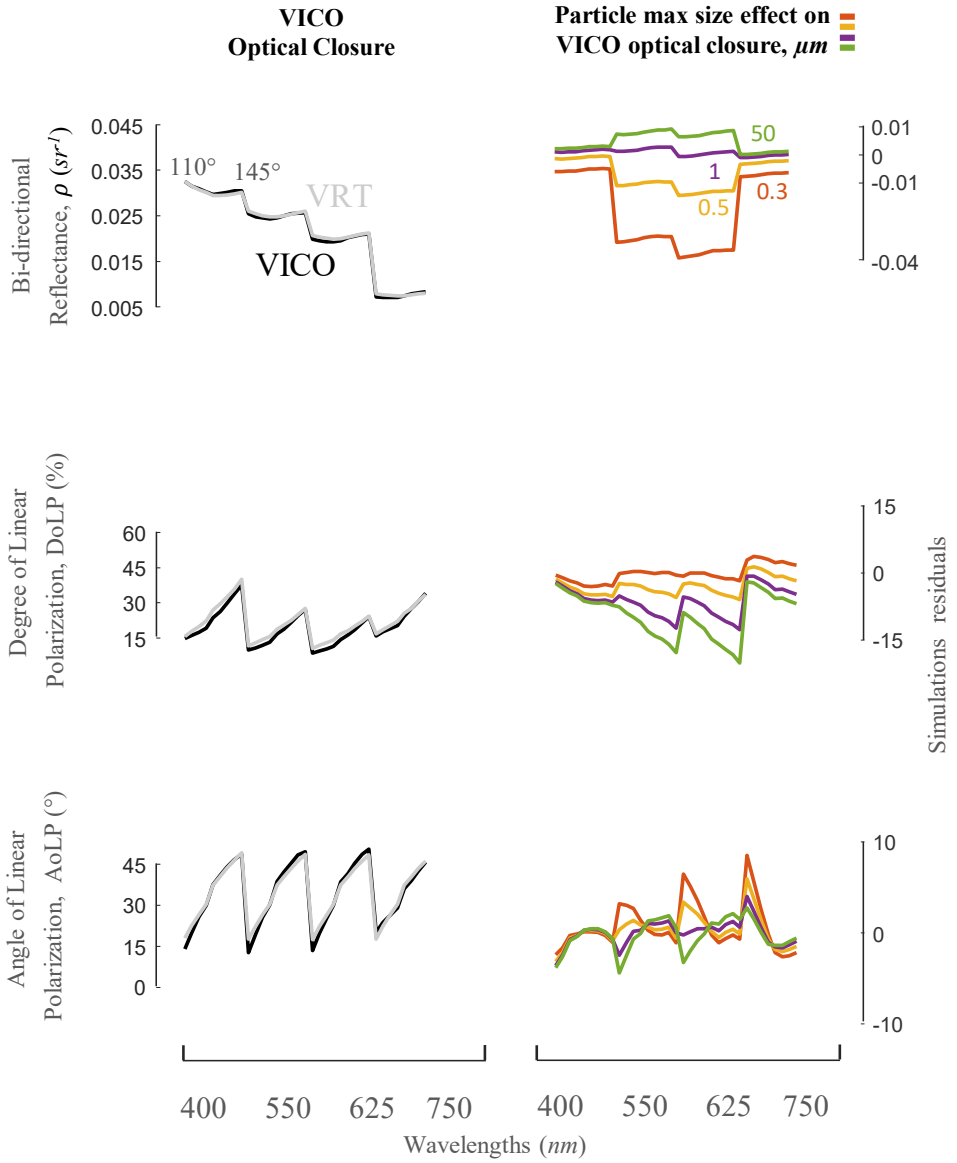

Fig. 3 Impact of hydrosol particles sizes (super- and sub-microns) on polarized optical closure at 1500 m altitude using VICO over coastal water. *Left column* shows the polarized optical closure (Measured vs Modeled). *Right column* shows the impact of hydrosol particles maximum size on the polarized closure. Results are shown for Reflectance, DoLP and AoLP at different scattering angles and wavelengths.

3.2 Jacobian sensitivity analysis of aerosol and hydrosol macro- and micro-physics

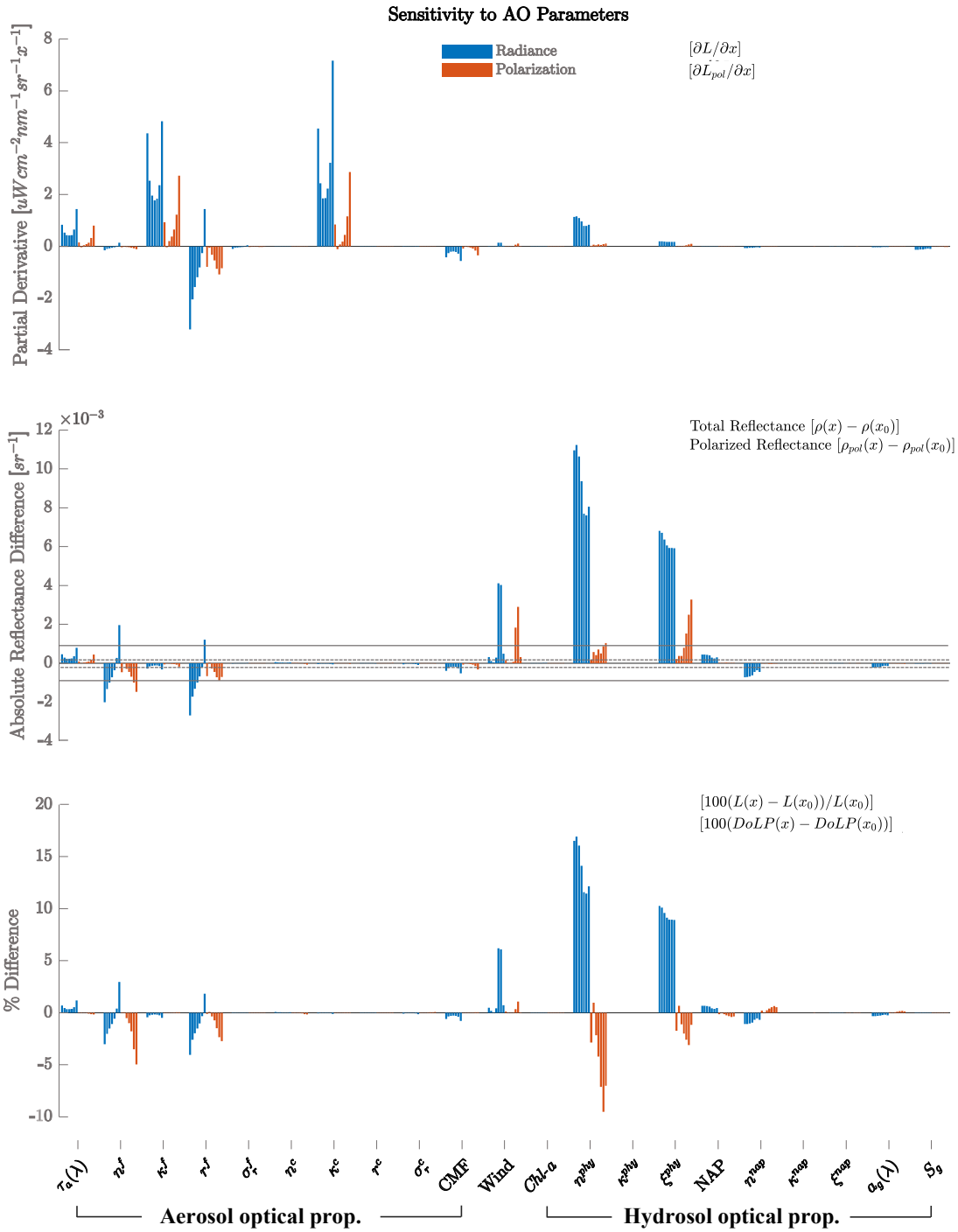

Fig. 4. Aircraft sensitivity analysis of Jacobian caused by 35% change in each aerosol and hydrosol microphysical parameter. The three panels show radiance and polarization sensitivity of all parameters. *Top panel* shows the partial derivative given in units of $\mu W\ cm^{-2}\ nm^{-1}\ sr^{-1}\ x^{-1}$ where x represents each of the microphysical parameter. *Middle panel* shows absolute reflectance difference given in units of sr^{-1} unit. *Bottom panel* shows relative difference given in units of *percent %*. Dash and solid gray lines in the middle plot are the polarimetric accuracy limits of the spaceborne POLDER sensor $|\rho_p| > 8.5 \times 10^{-4}\ sr^{-1}$ and of currently achievable accuracies $|\rho_p| > 1 \times 10^{-4}\ sr^{-1}$.

El-Habashi et. al. 2021 showed the polarized reflectance (ρp) could be significantly sensitive to the hydrosols at the blue band across most viewing angles. Again, this is because of the higher amount of the scattering processes produced by the suspended particulate matter, especially in coastal regions. The relevant geometries to simultaneously derive information on the aerosols' optical properties were also pointed out. In this section we investigate a Jacobian sensitivity analysis of aerosol and hydrosol microphysical parameters to the observed radiance and linear polarization at the blue band (443 nm) with nadir angles varied from -60° to 60° at 10° steps where the negative angles are in the direction toward Sun. A recursive VRT simulations were performed to estimate the Jacobian and its significance in several aerosol and hydrosol microphysical parameters simultaneously. The investigated aerosol parameters are total optical thickness, the volumetric radii r_V , standard deviations, σ_V, and complex aerosol refractive indices, m of the fine and coarse mode sized aerosols. The coarse to fine mode fraction is also included. The hydrosol parameters are concentrations, Junge slopes, complex refractive indices of the algae and non-algal particles as well as the spectral slope and blue absorption (440 nm) of the dissolved matters.

Figure 4 shows the aircraft radiance and polarization Jacobian sensitivity caused by 35% change in each aerosol and hydrosol microphysical parameter. The partial derivatives given in units of $\mu W\, cm^{-2}\, nm^{-1}\, sr^{-1}\, x^{-1}$ where x represents each microphysical parameter. The absolute reflectance difference and relative difference are also given in units of sr^{-1} and percent % respectively. The polarimetric accuracy limits of the spaceborne POLDER sensor ($|\rho_p| > 8.5 \times 10^{-4}$ sr $^{-1}$) and of currently achievable accuracies ($|\rho_p| > 1 \times 10^{-4}$ sr $^{-1}$) are shown as dash and solid gray lines in the middle plot of figure 4. Table 1 shows the top of the atmosphere highest reflectance difference caused by 10% change in each aerosol and hydrosol microphysical parameter. The highest reflectance differences are shown for each parameter with the related viewing geometry.

	Optical Properties		Value (10%)	TOA max. ρ difference (nadir angle)	
Aerosol	Optical thickness	$\tau_a(\lambda)$	$0.059\,(0.0059)$	2.40 x 10^{-3} (60°)	1.30 x 10^{-3} (60°)
	Fine mode real ref. index	n^f	$1.47\,(0.147)$	1.54 x 10^{-3} (60°)	-6.28 x 10^{-4} (60°)
	Fine mode img. ref. index	κ^f	$-0.007\,(-0.0007)$	-2.94x 10^{-4} (60°)	-1.65x 10^{-4} (60°)
	Fine mode radius	r^f	$0.09\,(0.009)$	-3.97x 10^{-3} (-60°)	-1.20x 10^{-3} (60°)
	Fine mode SD	σ_r^f	$0.02\,(0.002)$	-1.96x 10^{-5} (-60°)	-6.77x 10^{-6} (60°)
	Coarse mode real ref. index	n^c	$1.53\,(0.153)$	1.05x 10^{-3} (60°)	-1.05x 10^{-4} (60°)
	Coarse mode img. ref. index	κ^c	$-0.001\,(-0.0001)$	-5.57x 10^{-5} (60°)	-1.560x 10^{-5} (60°)
	Coarse mode radius	r^c	$3.2\,(0.32)$	-1.00x 10^{-5} (-60°)	1.90x 10^{-5} (60°)
	Coarse mode SD	σ_r^c	$0.75\,(0.075)$	-4.44x 10^{-5} (-60°)	2.80x 10^{-5}(60°)
	Coarse mode Fraction	CMF	$0.1\,(0.01)$	-1.10x 10^{-3} (60°)	-6.45x 10^{-4}(60°)
		Wind	$3\,(0.3)$	8.42x 10^{-4} (-60°)	5.42x 10^{-4} (40°)
Hydrosol	Chlorophyll-a particles conc.	$Chl\text{-}a$	$19\,(1.9)$	1.40x 10^{-6} (60°)	5.91x 10^{-7} (40°)
	Chlorophyll-a real ref. index	n^{phy}	$1.04\,(0.104)$	1.60x 10^{-3} (60°)	6.00x 10^{-4} (60°)
	Chlorophyll-a img. ref. index	κ^{phy}	$-2.77739e-11\,(-2.77739e-12)$	-	-
	Chlorophyll-a particles slope	ξ^{phy}	$3.7\,(0.37)$	3.68x 10^{-4} (-40°)	1.76x 10^{-4} (-60°)
	Minerals particles conc.	NAP	$21.8\,(2.18)$	1.12x 10^{-4} (-40°)	6.70x 10^{-6} (-60°)
	Minerals real ref. index	n^{nap}	$1.22\,(0.122)$	-2.57x 10^{-4} (-40°)	-1.54x 10^{-5} (-60°)
	Minerals img. ref. index	κ^{nap}	$-0.02\,(-0.002)$	-	-
	Minerals particles slope	ξ^{nap}	$3.7\,(0.37)$	-	-
	Dissolved matters abs.	$a_g(\lambda)$	$0.673\,(0.0673)$	-5.62x 10^{-5} (-40°)	-7.56x 10^{-6} (60°)
	Dissolved matters abs. slope	S_g	$0.014\,(0.0014)$	-4.18x 10^{-6} (-20°)	-5.06x 10^{-7} (60°)

Table 1. Top of the Atmosphere sensitivity analysis of Jacobian caused by 10% change in each aerosol and hydrosol microphysical parameter.

As expected, the principal plane measurements are essential for aerosol and cloud polarimetry to maximize the range of scattering angles. Off-glint geometries (~30 ° to 60° azimuth angle) are more useful

for ocean polarimetry to reduce the glint-contaminated pixels while still having a sufficient upwelling polarized signal to detect small- scale variations of the polarized light in the ocean.

4. ARCTIC AND ANTI-ARCTIC OCEAN -INHERENT OPTICAL PROPERTIES

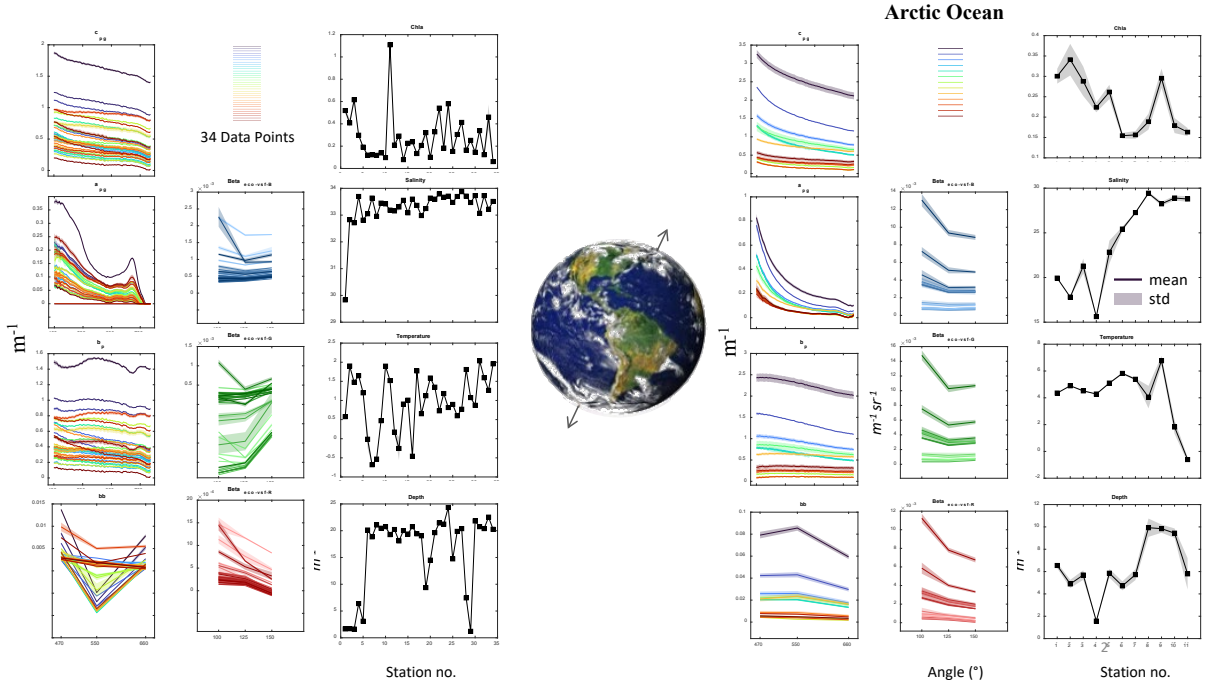

Fig. 5 Preliminary results of the inherent optical properties in the Arctic and Anti-Arctic oceans.

Arctic and Ant-Arctic are rapidly changing due to climate change. Remote sensing from space is useful tool to monitor these changes, however, the increased cloud cover and low sun angles in polar regions hinder the use of satellite remote sensing or current established retrieval algorithms in these areas. In situ optical and biological observations are needed to characterize the oceans in polar regions and correct the polar ocean retrievals from space. In this work, we provide a description of bio-optical properties of surface waters within the Arctic and Ant-Arctic oceans (Figure 5). Arctic and Ant-Arctic exhibit unique bio-optical properties that differ significantly from the global ocean. First, the Arctic is a spatially heterogeneous sea covered by a thin layer of sea ice and surrounded by land. The Arctic Ocean receives a large amount of fresh water through numerous rivers runoff relative to its area, compared to the Ant-Arctic and other oceans. This could be seen in the low values observed in the Arctic Salinity plot in Fig. 5. The Arctic sea vary with the different rivers inflow, nutrient availability, sea ice coverage, shelf width, and circulation patterns, which result in sub-regional differences with different CDOM and Chlorophyll concentration within the Arctic ocean. On the other hand, the Ant-Arctica is covered by a thick ice cap and surrounded by a rim of sea ice and the Southern Ocean. Figure 5 shows higher chlorophyll concentrations and particulate absorption and lower backscattering spectra in the Anti-Arctic compare to the Arctic ocean.

Polar phytoplankton acclimate to low light conditions by increasing chlorophyll-a content per cell resulting in increasing light absorbed per phytoplankton cell compared to the lower latitude phytoplankton's [14]. Therefore, Chlorophyll global algorithms underestimate Chlorophyll distributions in the polar regions, thus it is important to characterize bio-optical properties in the Arctic and Ant-Arctic oceans.

5. OCEAN MICRO-PLASTICS -INHERENT OPTICAL PROPERTIES

Multidecadal increase in plastic particles in coastal ocean sediments is persistent and seemingly ubiquitous, meanwhile microplastics IOP libraries are sparse and still in its exploratory phase. Performed laboratory work to characterize the hyperspectral Inherent Optical Properties, IOP of seven microplastics assemblages (synthetic polymers), commonly found in the marine environment. In here we performed laboratory work to characterize the hyperspectral Inherent Optical Properties, IOP of seven microplastics assemblages (synthetic polymers), commonly found in the marine environment. The goal is to improve radiative transfer simulations of microplastics in ocean for potential satellite detection limitations.

The AC-s meter are used to characterize the particulate spectral absorption and attenuation (a_{gp} and c_{gp}, m^{-1}) of each micro-plastic sample from 400 to 735nm spectral range. The measurements steps of each samples were as follow: Milli-Q was settled in a tank before use for at least 24 hours to get rid of any bubbles. A pure water baseline was made for AC-s meter at the start and end of each instrument run. No significant difference was observed between baselines. Fresh Milli-Q water was used to rinse absorption and attenuation tubes before measuring each sample. Moderate pressure was applied while rinsing AC-s tubes to ensure that optics and pathlength are sufficiently clean before each sample. Each sample was gently poured in the AC-s meter tubes. The AC-s is move slowly after pouring each sample to ensure adequate mixing of each sample. To prevent air bubbles during measurements, the AC-s meter was mounted approximately 45 degrees position. Data were recorded for approximately 3 minutes with at 5 Hz sample rate. Means and standard deviation of approximately 1000 data record were calculated for each parameter.

Data were extracted and temperature and scattering corrections were applied following the AC-s processing protocol. Pure water was subtracted to retrieve the particulate absorption, attenuation, scattering, and single scattering albedo. Preliminary results are shown in Fig. 6 and 7.

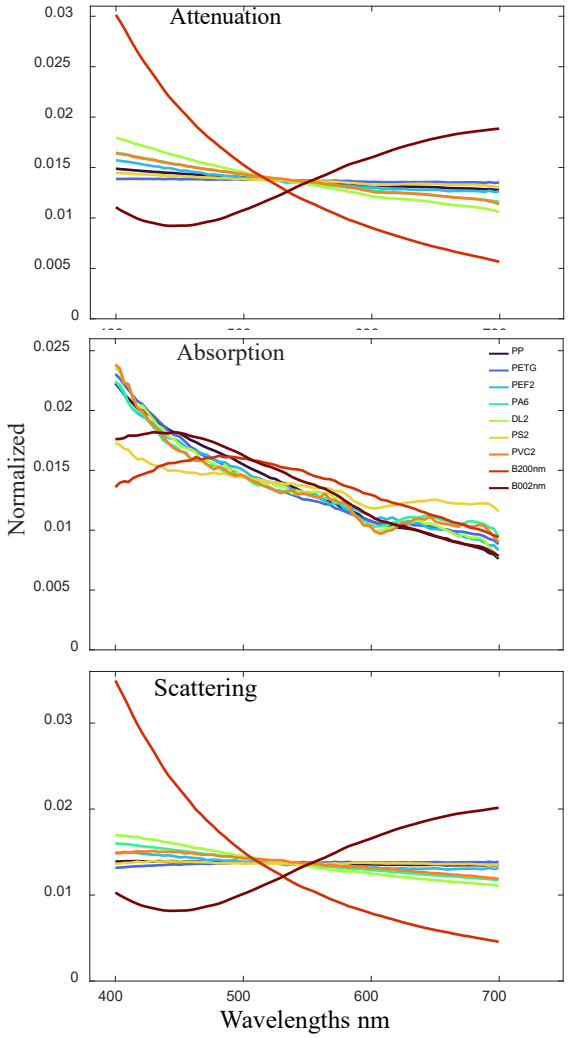

Fig. 6 Hyperspectral attenuation, absorption, and scattering for seven microplastics assemblages, commonly found in the marine environment. Results are compared to spherical particles standards of 200 and 2 nm size (B200 and B002).

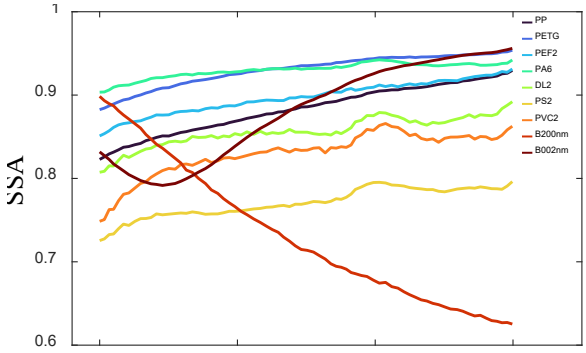

Fig. 7 Single Scattering Albedo for the seven microplastics assemblages and spherical particles standards in Fig. 6

6. SUMMARY

First, the impact of super- and sub-micron hydrosol particles on polarimetric optical closure were investigated for 0.3, 0.5, 1, 50 μm particles size limits. The corresponding variations due to the particles size limits ranged from 0.01 to -0.04 sr^{-1}, -1 to -20 %, 7 to -3 ° for the total reflectance ρ, Degree of Linear Polarization *DoLP*, and Angle of Linear Polarization *AoLP* respectively.

Second, a recursive VRT simulations were performed to determine the Jacobian and its significance in several aerosol and hydrosol microphysical parameters simultaneously. The sensitivity in radiance and linear polarization caused by 35% and 10% change in each aerosol and hydrosol microphysical parameter were calculated at the aircraft level (1500 *meter*) and at the top of the atmosphere (TOA), respectively. Analysis were made at the blue band (443 *nm*) with nadir angles varied from -60° to 60° at 10° steps. The viewing geometry with highest polarized reflectance difference were outlined for each parameter.

Third, Arctic and Anti-Arctic inherent optical properties were briefly shown, highlighting the differences and challenges in the two polar regions. Higher chlorophyll content and lower backscattering spectra is observed in the Anti-Arctic compare to the Arctic ocean.

Finally, optical properties, IOP of seven microplastics assemblages (synthetic polymers), commonly found in the marine environment were characterized with the goal to improve radiative transfer simulations of microplastics in ocean for potential satellite detection limitations

ACKNOWLEDGMENTS

Many thanks to several people for their support, assistance, and willingness to include me in their research: Dr. Jeffrey Bowles (NRL), Dr. Robert Foster (NRL), Dr. Deric Gray (NRL), Dr. Steve Ackleson (NRL), Dr. Wes Moses (NRL), Dr. Daniel Koestner (formerly NRL, now University of Bergen, Norway), and Dr. Kirk Knobelspiesse (NASA Goddard Space Flight Center).

REFERENCES

1. Foster, R., et al., *Hydrosol Scattering Matrix Inversion Across a Fresnel Boundary.* 2022. **2**: p. 791048.
2. Hansen, J.E. and L.D. Travis, *Light scattering in planetary atmospheres.* Space science reviews, 1974. **16**(4): p. 527-610.
3. Mishchenko, M.I., et al., *Monitoring of aerosol forcing of climate from space: analysis of measurement requirements.* Journal of Quantitative Spectroscopy and Radiative Transfer, 2004. **88**(1-3): p. 149-161.
4. El-Habashi, A., et al., *Polarized observations for advanced atmosphere-ocean algorithms using airborne multi-spectral hyper-angular polarimetric imager.* Journal of Quantitative Spectroscopy and Radiative Transfer, 2021. **262**: p. 107515.
5. Bowles, J.H., et al., *Airborne system for multispectral, multiangle polarimetric imaging.* Applied optics, 2015. **54**(31): p. F256-F267.
6. Thuillier, G., et al., *The solar spectral irradiance from 200 to 2400 nm as measured by the SOLSPEC spectrometer from the ATLAS and EURECA missions.* Solar Physics, 2003. **214**(1): p. 1-22.
7. Chowdhary, J., et al., *Testbed results for scalar and vector radiative transfer computations of light in atmosphere-ocean systems.* Journal of Quantitative Spectroscopy and Radiative Transfer, 2020. **242**: p. 106717.

8. Deuzé, J.-L., et al., *Fourier series expansion of the transfer equation in the atmosphere-ocean system.* Journal of Quantitative Spectroscopy and Radiative Transfer, 1989. **41**(6): p. 483-494.
9. Lenoble, J., et al., *A successive order of scattering code for solving the vector equation of transfer in the earth's atmosphere with aerosols.* Journal of Quantitative Spectroscopy and Radiative Transfer, 2007. **107**(3): p. 479-507.
10. Chami, M., et al., *OSOAA: a vector radiative transfer model of coupled atmosphere-ocean system for a rough sea surface application to the estimates of the directional variations of the water leaving reflectance to better process multi-angular satellite sensors data over the ocean.* Optics Express, 2015. **23**(21): p. 27829-27852.
11. Chowdhary, J., et al., *Retrieval of aerosol properties over the ocean using multispectral and multiangle photopolarimetric measurements from the Research Scanning Polarimeter.* Geophysical research letters, 2001. **28**(2): p. 243-246.
12. Mishchenko, M.I., L.D. Travis, and A.A. Lacis, *Scattering, absorption, and emission of light by small particles*. 2002: Cambridge university press.
13. Organelli, E., et al., *The open-ocean missing backscattering is in the structural complexity of particles.* 2018. **9**(1): p. 1-11.
14. Zhang, X., et al., *Experimental estimates of optical backscattering associated with submicron particles in clear oceanic waters.* 2020. **47**(4): p. e2020GL087100.

ACRONYMS

AoLP Angle of Linear Polarization. 2,3

CZCS Coastal Zone Color Scanner Experiment. 1

DoLP Degree of Linear Polarization. 2,3

[I, Q, U] Linear Stokes parameters of the incoming light

MISR Multi-angle Imaging SpectroRadiometer. 1

NASA National Aeronautics and Space Administration. 9

NRC National Research Council. E-1

POLDER POLarization and Directionality of the Earth's Reflectances. 6

ρ Reflectance. 2,3

TOA Top of the atmosphere. 2, 9

VICO Versatile Imager for the Coastal Ocean. 1-7, E-1